

Characteristic energy of the nematic-order state and its connection to enhancement of superconductivity in cuprate superconductors

Zhangkai Cao¹, Xingyu Ma¹, Yiqun Liu², Huaiming Guo³, and Shiping Feng^{1*}

¹*Department of Physics, Beijing Normal University, Beijing 100875, China*

²*School of Physics, Nanjing University, Nanjing 210093, China and*

³*School of Physics, Beihang University, Beijing 100191, China*

The new development in sublattice-phase-resolved imaging of electronic structure now allow for the visualisation of the nematic-order state characteristic energy of cuprate superconductors in a wide doping regime. However, it is still unclear how this characteristic energy of the nematic-order state is correlated with the enhancement of superconductivity. Here the doping dependence of the nematic-order state characteristic energy in cuprate superconductors and of its possible connection to the enhancement of superconductivity is investigated within the framework of the kinetic-energy-driven superconductivity. It is shown that the characteristic energy of the nematic-order state is found to be particularly large in the underdoped regime, then it smoothly decreases upon the increase of doping, in full agreement with the corresponding experimental observations. Moreover, the characteristic energy of the nematic-order state as a function of the nematic-order state strength in the underdoped regime presents a similar behavior of the superconducting transition temperature. This suggests a possible connection between the nematic-order state characteristic energy and the enhancement of the superconductivity.

PACS numbers: 74.25.Jb, 74.25.Dw, 74.20.Mn, 74.72.-h

I. INTRODUCTION

In cuprate superconductors¹, the strongly correlated motion of the electrons is confined to the square-lattice CuO₂ planes^{2,3}. However, this strong electron correlation also induces the system to exhibit numerous ordering tendencies⁴⁻⁹. In addition to superconductivity, a variety of spontaneous symmetry-breaking orders have been observed experimentally, indicating the coexistence and intertwinement between these spontaneous symmetry-breaking orders and superconductivity⁴⁻⁹. Among these spontaneous symmetry-breaking orders, the most distinct form of order is electronic nematicity⁶⁻⁹, which corresponds to that the electronic structure preserves the translation symmetry but breaks the rotation symmetry of the underlying square-lattice CuO₂ plane. This is why in the common practice, the *strength of the electronic nematicity* is defined as the *orthorhombicity of the electronic structure*¹⁰. As a natural consequence of a doped Mott insulator, the manipulation of the particular characteristics of the superconducting (SC) state with coexisting electronically nematic order through the control of the doping and strength of the electronic nematicity is hotly debated and has been believed to be key to the understanding of the problem of why cuprate superconductors exhibit a number of the anomalous properties⁴⁻⁹.

Experimentally, the multiple measurement techniques have been used to elucidate the nature of the quasiparticle excitation and of its interplay with spontaneous symmetry-breaking orders and superconductivity¹⁰⁻²⁶, where it has been found that the electronically nematic order coexists with the translation symmetry breaking such as charge order (or equivalently charge density wave) in the well-defined regimes of the phase diagrams, appearing below the pseudogap crossover temperature T^*

in the underdoped regime, and coexists with charge order and superconductivity below the SC transition temperature T_c . It thus shows that the electronic nematicity is an integral part of the essential physics of cuprate superconductors. The temperature scale for the onset of the dynamical charge order may increase monotonically with the decrease of doping in the underdoped regime, however, the static charge order may exhibit a dome-like shape temperature dependence²¹⁻²⁶. In particular, this interplay of the electronically nematic order and charge order in the normal-state has been invoked recently to give a consistent explanation of the transport anisotropy²⁷. However, although a number of consequences from the electronic nematicity together with the associated fluctuation phenomena have been identified in the early experimental measurements¹⁰⁻²⁰, the evolution of the characteristic quantities of the electronic nematicity itself with doping in the entire range of the SC dome remains puzzling. Fortunately, the instrumentation for sublattice-phase-resolved imaging of electronic structure has improved dramatically in recent years, allowing this experimental technique to visualize simultaneously the doping and energy dependence of the quasiparticle scattering interference (QSI) in the SC-state with coexisting symmetry-breaking ordered states²⁸. In this case, as a compensation for the early scanning tunneling spectroscopy (STS) experimental studies¹⁸⁻²⁰, this experimental technique has been used to detect the doping and energy dependence of the tunneling conductance of Bi₂Sr₂CaCu₂O_{8+δ} over a large field of view, perform a Fourier transform, and analyze data from distinct regions of momentum space²⁸. Moreover, to establish the link between the pseudogap and electronic nematicity, the doping and energy dependence of the averaged density of states $\rho(E)$ and the doping and energy dependence

of the nematic-order spectrum,

$$N^{(Z)}(E) = \text{Re}Z(\mathbf{Q}_y^{(B)}, E) - \text{Re}Z(\mathbf{Q}_x^{(B)}, E), \quad (1)$$

in momentum space from the reciprocal lattice vectors $\mathbf{Q}_x^{(B)} = [2\pi, 0]$ and $\mathbf{Q}_y^{(B)} = [0, 2\pi]$ have been measured²⁸, where $Z(\mathbf{r}, E) \equiv g(\mathbf{r}, E)/g(\mathbf{r}, -E)$ is a ratio of differential tunneling conductances at opposite bias, while $g(\mathbf{r}, E) = dI(\mathbf{r}, E = eV)/dV$ is differential tunneling conductance. This nematic-order spectrum $N^{(Z)}(E)$ can be also defined as the *order parameter of the electronic nematicity*²⁰. The pseudogap extracted directly from the measured data of the averaged density of states shows that the pseudogap smoothly decreases upon the increase of doping²⁸. On the other hand, the measured data of the order parameter of the electronic nematicity $N^{(Z)}(E)$ show that $N^{(Z)}(E)$ has a dome-like shape energy dependence²⁸, with the maximal $N^{(Z)}(E)$ appearance at an energy $E_{\text{max}}^{(N)}$. This energy $E_{\text{max}}^{(N)}$ associated with the maximal $N^{(Z)}(E)$ is so-called the *nematic-order state characteristic energy*. More importantly, the evolution of the nematic-order state characteristic energy with doping is identified, where measured on the samples whose doping spans the pseudogap regime, the nematic-state characteristic energy $E_{\text{max}}^{(N)}$ and pseudogap energy $\bar{\Delta}_{\text{PG}}$ are, within the experimental error, identical²⁸. These experimental results therefore identify the electronically nematic order exists across the entire range of the SC dome. On the basis of these experimental results, it has been argued that the pseudogap is a consequence of a tendency towards an electronically ordered state that is a coexistence of the nematic order and charge orders and breaks both the translation and rotation symmetry^{6,28}.

Although the doping dependence of the nematic-order state characteristic energy in cuprate superconductors has been well-identified experimentally in the entire range of the SC dome²⁸, its full understanding is still a challenging issue. In particular, it is still unclear how this nematic-order state characteristic energy $E_{\text{max}}^{(N)}$ evolves with the strength of the electronic nematicity. Theoretically, the possible origins of the emergence of the electronic nematicity have been suggested: the electronically nematic order occurs upon melting of stripe order or charge order^{29–32}, or induces by the electron Fermi surface (EFS) instability^{33,34}, or is attributed to the incommensurate pair-density-wave^{35,36}. In particular, it has been proposed that the density of states near EFS and geometry of EFS (then the band structure) strongly affect the nematic-order formation^{37,38}. This follows a basic fact that in the square-lattice CuO_2 planes, both the density of states near EFS and geometry of EFS change significantly when the quasiparticle dispersion possesses a saddle point induced by the van Hove singularity. In our recent study³⁹, the intertwinement of the electronic nematicity with superconductivity in cuprate superconductors has been studied based on the kinetic-energy-driven superconductivity, where we have shown that the electronic nematicity enhances superconductivity. Moreover,

we³⁹ have also shown that the order parameter of the electronic nematicity achieves its maximum in the characteristic energy of the nematic-order state, and then decreases rapidly as the energy moves away from the characteristic energy of the nematic-order state, in agreement with the experimental observation²⁸. However, a natural question is whether the characteristic energy of the nematic-order state is correlated with the enhancement of superconductivity or not? In this paper, we study the doping dependence of the nematic-order state characteristic energy and of its possible connection to the enhancement of superconductivity along with this line, where one of our main results is that both the characteristic energy of the nematic-order state and enhancement of T_c exhibit the same nematic-order state strength dependence, i.e., the maximal characteristic energy of the nematic-order state (then the maximal T_c) occurs at around the optimal strength of the electronic nematicity, and then decreases in both weak and strong strength regions. This suggests a possible connection between the characteristic energy of the nematic-order state and the enhancement of superconductivity.

This paper is organized as follows. We present the basic formalism in Sec. II, and then discuss the doping dependence of the nematic-order state characteristic energy and of its possible connection to the enhancement of superconductivity in Sec. III, where we show that in a striking similar to the doping dependence of the pseudogap state, the nematic-order state is particularly obvious in the underdoped regime, i.e., the characteristic energy of the nematic-order state is particularly large in the underdoped regime, and then it monotonically decreases with the increase of doping, in full agreement with the corresponding experimental observations²⁸. Finally, we give a summary and discussions in Sec. IV.

II. MODEL AND THEORETICAL METHOD

When the quasiparticle scattering mixes the states \mathbf{k} and $\mathbf{k} + \mathbf{q}$, a QSI pattern with the wave vector \mathbf{q} appears in the norm of the quasiparticle wave function and the local density of states modulations with the wave length $\lambda = 2\pi/|\mathbf{q}|$ appear, reflecting a basic fact that the QSI pattern manifests itself is an autocorrelation between the quasiparticle bands $E_{\mathbf{k}}$ and $E_{\mathbf{k}+\mathbf{q}}$ ^{40–42}. In other words, the intensity in the QSI pattern is proportional to the spectral intensities of the single-particle excitation spectra at the momenta \mathbf{k} and $\mathbf{k} + \mathbf{q}$, while the sharp intensity peaks in the QSI pattern then are corresponding to the highest joint density of states. This is why the quasiparticle scattering processes, the quasiparticle momentum-space structure, and the dispersion of the peaks in the QSI pattern as a function of energy are interpreted in terms of the octet scattering model^{43,44}, and yields the crucial information of the quasiparticle excitation. More importantly, by the analysis of the typical feature of the Bragg peaks in a QSI pattern, one is considering the phe-

nomena that occur with the periodicity of the underlying square lattice and which qualify any rotation symmetry-breaking^{40–42}. Likewise, the autocorrelation between the quasiparticle bands $E_{\mathbf{k}}$ and $E_{\mathbf{k}+\mathbf{q}}$ can be also measured in terms of the angle-resolved photoemission spectroscopy (ARPES) autocorrelation⁴⁵,

$$\bar{C}_\zeta(\mathbf{q}, \omega) = \frac{1}{N} \sum_{\mathbf{k}} I_\zeta(\mathbf{k} + \mathbf{q}, \omega) I_\zeta(\mathbf{k}, \omega), \quad (2)$$

where N is the number of lattice sites, and $I_\zeta(\mathbf{k}, \omega)$ is the single-particle excitation spectrum, while the summation of momentum \mathbf{k} is extended up to the second Brillouin zone (BZ)⁴⁵ for the discussion of QSI together with the Bragg scattering. This ARPES autocorrelation in Eq. (2) describes the correlation of the spectral intensities of the single-particle excitation spectra at two different momenta \mathbf{k} and $\mathbf{k} + \mathbf{q}$, separated by a momentum transfer \mathbf{q} , at a fixed energy, and is effectively the momentum-resolved joint density of states. In particular, it has been demonstrated experimentally^{45,46} that the peaks, the momentum-space structure, and the dispersion of the peaks in the ARPES autocorrelation pattern are directly related to the peaks, the momentum-space structure, and the dispersion of the peaks in the QSI pattern^{40–42}, respectively, and can be also explained straightforwardly in terms of the octet scattering model⁴³. This is why the characteristic features of QSI can be also obtained in terms of the ARPES autocorrelation.

The single-particle excitation spectrum $I_\zeta(\mathbf{k}, \omega)$ in Eq. (2) is proportional to the electron spectral function $A_\zeta(\mathbf{k}, \omega)$ as,

$$I_\zeta(\mathbf{k}, \omega) \propto n_F(\omega) A_\zeta(\mathbf{k}, \omega), \quad (3)$$

where $n_F(\omega)$ is the fermion distribution, while the electron spectral function $A_\zeta(\mathbf{k}, \omega)$ in the SC-state with coexisting electronic nematicity can be obtained directly from the full electron diagonal propagator as $A_\zeta(\mathbf{k}, \omega) = -2\text{Im}G_\zeta(\mathbf{k}, \omega)$.

Now our goal is to evaluate this full electron diagonal propagator $G_\zeta(\mathbf{k}, \omega)$ starting from a microscopic SC theory. The strongly correlated motion of the electrons in cuprate superconductors is restricted to the square-lattice CuO_2 planes^{2,3} as mentioned above, and then the unconventional properties come from the strongly correlated motion of the electrons in these CuO_2 planes. In particular, as originally emphasized by Anderson⁴⁷, the essential physics of the strongly correlated motion of the electrons in a square-lattice CuO_2 plane can be described properly by the t - J model,

$$H = - \sum_{l\hat{\eta}\sigma} t_{\hat{\eta}} C_{l\sigma}^\dagger C_{l+\hat{\eta}\sigma} + \sum_{l\hat{\tau}\sigma} t'_{\hat{\tau}} C_{l\sigma}^\dagger C_{l+\hat{\tau}\sigma} + \mu \sum_{l\sigma} C_{l\sigma}^\dagger C_{l\sigma} + \sum_{l\hat{\eta}} J_{\hat{\eta}} \mathbf{S}_l \cdot \mathbf{S}_{l+\hat{\eta}}, \quad (4)$$

where $\hat{\eta} = \pm\hat{x}, \pm\hat{y}$ represents the nearest neighbor (NN) sites of a given site l , $\hat{\tau} = \pm\hat{x} \pm \hat{y}$ represents the next

NN sites of a given site l , $C_{l\sigma}^\dagger$ and $C_{l\sigma}$ are the electron creation and annihilation operators, respectively, \mathbf{S}_l is the spin operator with its components S_l^x , S_l^y , and S_l^z , while μ is the chemical potential. For the discussions of the exotic features of the SC-state with coexisting electronic nematicity, the next NN hopping amplitude in the t - J model (4) is chosen as $t'_{\hat{\tau}} = t'$, while the NN hopping amplitude $t_{\hat{\eta}}$ has the following form¹⁰,

$$t_{\hat{x}} = (1 - \zeta)t, \quad t_{\hat{y}} = (1 + \zeta)t, \quad (5)$$

which is strongly anisotropic along the \hat{x} and \hat{y} directions and follows from the previous analyses of the exotic features in the nematic-order state^{48–51}. In particular, this anisotropic NN hopping amplitude in Eq. (5) has been experimentally verified in terms of the standard tight-binding model to fit the ARPES spectrum in the nematic-order state¹⁰. Concomitantly, this anisotropic NN hopping amplitude in Eq. (5) induces the anisotropic NN exchange coupling $J_{\hat{x}} = (1 - \zeta)^2 J$ and $J_{\hat{y}} = (1 + \zeta)^2 J$ in the t - J model (4). Moreover, *this anisotropic parameter ζ in Eq. (5) represents the orthorhombicity of the electronic structure, and therefore can be defined as the strength of the electronic nematicity in the system*¹⁰. In this sense, the anisotropic NN hopping amplitudes in Eq. (5) also indicate that the rotation symmetry is broken already in the starting t - J model (4). In cuprate superconductors, although the values of J , t , and t' are believed to vary somewhat from compound to compound, the commonly used parameters in this paper are chosen as $t/J = 3$, $t'/t = 1/3$, and $J = 100$ meV as in our previous discussions³⁹. Moreover, the temperature T is set at $T = 0.002J$. Unless otherwise indicated, the doping is fixed at $\delta = 0.06$ for a direct comparison with the corresponding experimental result²⁸.

The t - J model (4) is supplemented by a on-site local constraint of no double electron occupancy^{52–54}, i.e., $\sum_{\sigma} C_{l\sigma}^\dagger C_{l\sigma} \leq 1$. However, the most difficult in the analytical treatment of the t - J model (4) comes mainly from this local constraint of no double electron occupancy, while the strong electron correlation manifests itself by this local constraint of no double electron occupancy, and therefore the crucial requirement is to impose this local constraint of no double electron occupancy. To incorporate this local constraint of no double electron occupancy, the fermion-spin transformation^{55,56} has been proposed, where the physics of no double electron occupancy is taken into account by representing the electron as a composite object created by,

$$C_{l\uparrow} = h_{l\uparrow}^\dagger S_l^-, \quad C_{l\downarrow} = h_{l\downarrow}^\dagger S_l^+, \quad (6)$$

with the spinful fermion operator $h_{l\sigma} = e^{-i\Phi_{l\sigma}} h_l$ that represents the charge degree of freedom of the constrained electron together with some effects of spin configuration rearrangements due to the presence of the doped hole itself (charge carrier), while the spin operator S_l describes the spin degree of freedom of the constrained electron, and then the local constraint of no double occupancy is satisfied in analytical calculations. In this

fermion-spin representation (6), the original t - J model in Eq. (4) can be rewritten as,

$$\begin{aligned}
H = & \sum_{l\hat{\eta}} t_{\hat{\eta}} (h_{l+\hat{\eta}\uparrow}^\dagger h_{l\uparrow} S_l^+ S_{l+\hat{\eta}}^- + h_{l+\hat{\eta}\downarrow}^\dagger h_{l\downarrow} S_l^- S_{l+\hat{\eta}}^+) \\
& - \sum_{l\hat{\tau}} t'_{\hat{\tau}} (h_{l+\hat{\tau}\uparrow}^\dagger h_{l\uparrow} S_l^+ S_{l+\hat{\tau}}^- + h_{l+\hat{\tau}\downarrow}^\dagger h_{l\downarrow} S_l^- S_{l+\hat{\tau}}^+) \\
& - \mu_h \sum_{l\sigma} h_{l\sigma}^\dagger h_{l\sigma} + \sum_{l\hat{\eta}} J_{\text{eff}}^{(\hat{\eta})} \mathbf{S}_l \cdot \mathbf{S}_{l+\hat{\eta}}, \quad (7)
\end{aligned}$$

where μ_h is the charge-carrier chemical potential, $S_l^- = S_l^x - iS_l^y$ and $S_l^+ = S_l^x + iS_l^y$ are the spin-lowering and spin-raising operators for the spin $S = 1/2$, respectively, $J_{\text{eff}}^{(\hat{\eta})} = (1 - \delta)^2 J_{\hat{\eta}}$, and $\delta = \langle h_{l\sigma}^\dagger h_{l\sigma} \rangle$ is the charge-carrier doping concentration.

Within the t - J model in the fermion-spin representation, the kinetic-energy-driven SC mechanism has been developed in the case of the absence of the electronic nematicity⁵⁶⁻⁵⁹, where the interaction between the charge carriers directly from the kinetic energy of the t - J model by the exchange of a strongly dispersive *spin excitation* generates the d-wave charge-carrier pairing in the particle-particle channel, then the d-wave electron pairs originated from the d-wave charge-carrier pairing state are due to the charge-spin recombination, and their condensation reveals the d-wave SC-state. The typical features of the kinetic-energy-driven superconductivity can be also summarized as: (i) the mechanism of the kinetic-energy-driven superconductivity is purely electronic without phonons; (ii) the mechanism of the kinetic-energy-driven superconductivity shows that the strong electron correlation is favorable to superconductivity, since the bosonic glue is identified into an electron pairing mechanism not involving the phonon, the external degree of freedom, but the internal spin degree of freedom of the constrained electron; (iii) the SC-state is controlled by both the SC gap and quasiparticle coherence, which leads to that the maximal T_c occurs around the optimal doping, and then decreases in both the underdoped and the overdoped regimes. Very recently, the framework of the kinetic-energy-driven superconductivity⁵⁶⁻⁵⁹

has been generalized to discuss the intertwinement of the electronic nematicity with superconductivity in cuprate superconductors³⁹, where the breaking of the rotation symmetry due to the presence of the electronic nematicity is verified by the inequivalence on the average of the electronic structure at the two Bragg scattering sites. Our following discussions builds on the work in Ref. 39, and only a short summary of the formalism is therefore given. In the recent discussions³⁹, the full electron diagonal and off-diagonal propagators of the t - J model (4) have been given explicitly as,

$$G_\zeta(\mathbf{k}, \omega) = \frac{1}{\omega - \varepsilon_{\mathbf{k}}^{(\zeta)} - \Sigma_{\text{tot}}^{(\zeta)}(\mathbf{k}, \omega)}, \quad (8a)$$

$$\mathfrak{G}_\zeta^\dagger(\mathbf{k}, \omega) = \frac{L_{\mathbf{k}}^{(\zeta)}(\omega)}{\omega - \varepsilon_{\mathbf{k}}^{(\zeta)} - \Sigma_{\text{tot}}^{(\zeta)}(\mathbf{k}, \omega)}, \quad (8b)$$

where the orthorhombic energy dispersion in the tight-binding approximation is obtained directly from the t - J model (4) as,

$$\varepsilon_{\mathbf{k}}^{(\zeta)} = -4t[(1 - \zeta)\gamma_{\mathbf{k}_x} + (1 + \zeta)\gamma_{\mathbf{k}_y}] + 4t'\gamma'_{\mathbf{k}} + \mu, \quad (9)$$

with $\gamma_{\mathbf{k}_x} = \cos k_x/2$, $\gamma_{\mathbf{k}_y} = \cos k_y/2$, $\gamma'_{\mathbf{k}} = \cos k_x \cos k_y$, while the total self-energy $\Sigma_{\text{tot}}^{(\zeta)}(\mathbf{k}, \omega)$ and weight function $L_{\mathbf{k}}^{(\zeta)}(\omega)$ are specific combinations of the normal self-energy $\Sigma_{\text{ph}}^{(\zeta)}(\mathbf{k}, \omega)$ in the particle-hole channel and anomalous self-energy $\Sigma_{\text{pp}}^{(\zeta)}(\mathbf{k}, \omega)$ in the particle-particle channel as,

$$\Sigma_{\text{tot}}^{(\zeta)}(\mathbf{k}, \omega) = \Sigma_{\text{ph}}^{(\zeta)}(\mathbf{k}, \omega) + \frac{|\Sigma_{\text{pp}}^{(\zeta)}(\mathbf{k}, \omega)|^2}{\omega + \varepsilon_{\mathbf{k}}^{(\zeta)} + \Sigma_{\text{ph}}^{(\zeta)}(\mathbf{k}, -\omega)}, \quad (10a)$$

$$L_{\mathbf{k}}^{(\zeta)}(\omega) = -\frac{\Sigma_{\text{pp}}^{(\zeta)}(\mathbf{k}, \omega)}{\omega + \varepsilon_{\mathbf{k}}^{(\zeta)} + \Sigma_{\text{ph}}^{(\zeta)}(\mathbf{k}, -\omega)}, \quad (10b)$$

where the normal self-energy $\Sigma_{\text{ph}}^{(\zeta)}(\mathbf{k}, \omega)$ and anomalous self-energy $\Sigma_{\text{pp}}^{(\zeta)}(\mathbf{k}, \omega)$ have been obtained in Ref. 39, and can be expressed explicitly as,

$$\begin{aligned}
\Sigma_{\text{ph}}^{(\zeta)}(\mathbf{k}, \omega) = & \frac{1}{2N^2} \sum_{\mathbf{p}\mathbf{p}'\nu} (-1)^{\nu+1} \Omega_{\mathbf{p}\mathbf{p}'\mathbf{k}}^{(\zeta)} \left[\left(1 + \frac{\bar{\varepsilon}_{\mathbf{p}+\mathbf{k}}^{(\zeta)}}{E_{\mathbf{p}+\mathbf{k}}^{(\zeta)}} \right) \left(\frac{F_{1\nu}^{(\zeta)}(\mathbf{p}, \mathbf{p}', \mathbf{k})}{\omega + \omega_{\zeta\mathbf{p}\mathbf{p}'}^{(\nu)} - E_{\mathbf{p}+\mathbf{k}}^{(\zeta)}} - \frac{F_{2\nu}^{(\zeta)}(\mathbf{p}, \mathbf{p}', \mathbf{k})}{\omega - \omega_{\zeta\mathbf{p}\mathbf{p}'}^{(\nu)} - E_{\mathbf{p}+\mathbf{k}}^{(\zeta)}} \right) \right. \\
& \left. + \left(1 - \frac{\bar{\varepsilon}_{\mathbf{p}+\mathbf{k}}^{(\zeta)}}{E_{\mathbf{p}+\mathbf{k}}^{(\zeta)}} \right) \left(\frac{F_{1\nu}^{(\zeta)}(\mathbf{p}, \mathbf{p}', \mathbf{k})}{\omega - \omega_{\zeta\mathbf{p}\mathbf{p}'}^{(\nu)} + E_{\mathbf{p}+\mathbf{k}}^{(\zeta)}} - \frac{F_{2\nu}^{(\zeta)}(\mathbf{p}, \mathbf{p}', \mathbf{k})}{\omega + \omega_{\zeta\mathbf{p}\mathbf{p}'}^{(\nu)} + E_{\mathbf{p}+\mathbf{k}}^{(\zeta)}} \right) \right], \quad (11a)
\end{aligned}$$

$$\begin{aligned}
\Sigma_{\text{pp}}^{(\zeta)}(\mathbf{k}, \omega) = & \frac{1}{2N^2} \sum_{\mathbf{p}\mathbf{p}'\nu} (-1)^\nu \Omega_{\mathbf{p}\mathbf{p}'\mathbf{k}}^{(\zeta)} \frac{\bar{\Delta}_{\zeta Z}(\mathbf{p} + \mathbf{k})}{E_{\mathbf{p}+\mathbf{k}}^{(\zeta)}} \left[\left(\frac{F_{1\nu}^{(\zeta)}(\mathbf{p}, \mathbf{p}', \mathbf{k})}{\omega + \omega_{\zeta\mathbf{p}\mathbf{p}'}^{(\nu)} - E_{\mathbf{p}+\mathbf{k}}^{(\zeta)}} - \frac{F_{2\nu}^{(\zeta)}(\mathbf{p}, \mathbf{p}', \mathbf{k})}{\omega - \omega_{\zeta\mathbf{p}\mathbf{p}'}^{(\nu)} - E_{\mathbf{p}+\mathbf{k}}^{(\zeta)}} \right) \right. \\
& \left. - \left(\frac{F_{1\nu}^{(\zeta)}(\mathbf{p}, \mathbf{p}', \mathbf{k})}{\omega - \omega_{\zeta\mathbf{p}\mathbf{p}'}^{(\nu)} + E_{\mathbf{p}+\mathbf{k}}^{(\zeta)}} - \frac{F_{2\nu}^{(\zeta)}(\mathbf{p}, \mathbf{p}', \mathbf{k})}{\omega + \omega_{\zeta\mathbf{p}\mathbf{p}'}^{(\nu)} + E_{\mathbf{p}+\mathbf{k}}^{(\zeta)}} \right) \right], \quad (11b)
\end{aligned}$$

where $\nu = 1, 2$, $\Omega_{\mathbf{p}\mathbf{p}'\mathbf{k}}^{(\zeta)} = Z_F^{(\zeta)} [\Lambda_{\mathbf{p}+\mathbf{p}'+\mathbf{k}}^{(\zeta)}]^2 B_{\mathbf{p}}^{(\zeta)} B_{\mathbf{p}+\mathbf{p}'}^{(\zeta)} / (4\omega_{\mathbf{p}}^{(\zeta)} \omega_{\mathbf{p}+\mathbf{p}'}^{(\zeta)})$ with $\Lambda_{\mathbf{k}}^{(\zeta)} = 4t[(1-\zeta)\gamma_{\mathbf{k}_x} + (1+\zeta)\gamma_{\mathbf{k}_y}] - 4t'\gamma'_{\mathbf{k}}$, the SC quasiparticle energy spectrum $E_{\mathbf{k}}^{(\zeta)} = \sqrt{\varepsilon_{\mathbf{k}}^{(\zeta)2} + |\bar{\Delta}_Z^{(\zeta)}(\mathbf{k})|^2}$ with the renormalized SC gap $\bar{\Delta}_Z^{(\zeta)}(\mathbf{k}) = Z_F^{(\zeta)} \bar{\Delta}^{(\zeta)}(\mathbf{k})$ and renormalized electron orthorhombic energy dispersion $\bar{\varepsilon}_{\mathbf{k}}^{(\zeta)} = Z_F^{(\zeta)} \varepsilon_{\mathbf{k}}^{(\zeta)}$, $\omega_{\mathbf{c}\mathbf{p}\mathbf{p}'}^{(\nu)} = \omega_{\mathbf{p}+\mathbf{p}'}^{(\zeta)} - (-1)^\nu \omega_{\mathbf{p}'}^{(\zeta)}$, while the quasiparticle coherent weight $Z_F^{(\zeta)}$, the SC gap $\bar{\Delta}^{(\zeta)}(\mathbf{k})$, the spin orthorhombic excitation spectrum $\omega_{\mathbf{k}}^{(\zeta)}$, the weight function of the spin excitation spectrum $B_{\mathbf{k}}^{(\zeta)}$, and the functions $F_{1\nu}^{(\zeta)}(\mathbf{p}, \mathbf{p}', \mathbf{k})$ and $F_{2\nu}^{(\zeta)}(\mathbf{p}, \mathbf{p}', \mathbf{k})$ have been given explicitly in Ref. 39. In particular, the sharp peak visible for temperature $T \rightarrow 0$ in the normal (anomalous) self-energy is actually a δ -function, broadened by a small damping used in the numerical calculation at a finite lattice. The calculation in this paper for the normal (anomalous) self-energy is performed numerically on a 120×120 lattice in momentum space, with the infinitesimal $i0_+ \rightarrow i\Gamma$ replaced by a small damping $\Gamma = 0.05J$.

With the above full electron diagonal Green's function (8a), the electron spectral function $A_c(\mathbf{k}, \omega)$ in the SC-state with coexisting electronic nematicity now can be obtained explicitly as,

$$A_\zeta(\mathbf{k}, \omega) = \frac{-2\text{Im}\Sigma_{\text{tot}}^{(\zeta)}(\mathbf{k}, \omega)}{[\omega - \varepsilon_{\mathbf{k}}^{(\zeta)} - \text{Re}\Sigma_{\text{tot}}^{(\zeta)}(\mathbf{k}, \omega)]^2 + [\text{Im}\Sigma_{\text{tot}}^{(\zeta)}(\mathbf{k}, \omega)]^2}, \quad (12)$$

where $\text{Re}\Sigma_{\text{tot}}^{(\zeta)}(\mathbf{k}, \omega)$ and $\text{Im}\Sigma_{\text{tot}}^{(\zeta)}(\mathbf{k}, \omega)$ are the real and imaginary parts of the total self-energy $\Sigma_{\text{tot}}(\mathbf{k}, \omega)$, respectively. Substituting this electron spectral function $A_\zeta(\mathbf{k}, \omega)$ in Eq. (12) into Eqs. (3) and (2), we therefore obtain the ARPES autocorrelation $\bar{C}_\zeta(\mathbf{q}, \omega)$ within the framework of the kinetic-energy-driven superconductivity.

III. QUANTITATIVE CHARACTERISTICS

In the presence of the electronic nematicity, the original electronic structure with the four-fold (C_4) rotation symmetry on the square lattice in the absence of the electronic nematicity is broken up into that with a residual two-fold (C_2) rotation symmetry, while such an aspect should be reflected in QSI. For convenience, we plot the ARPES autocorrelation $\bar{C}_\zeta(\mathbf{q}, \omega)$ in Fig. 1a. We are considering the binding-energy $\omega = 94$ meV and the strength of the electronic nematicity $\zeta = 0.006$. In Fig. 1a, the locations of the Bragg peaks $\mathbf{Q}_x^{(B)} = [\pm 2\pi, 0]$ along the \hat{x} axis and $\mathbf{Q}_y^{(B)} = [0, \pm 2\pi]$ along the \hat{y} axis are indicated by the circles, while $\mathbf{q}_1, \mathbf{q}_2, \mathbf{q}_3, \mathbf{q}_4, \mathbf{q}_5, \mathbf{q}_6,$ and \mathbf{q}_7 are different quasiparticle scattering wave vectors. For a better comparison, the corresponding experimental result²⁸ of the QSI pattern observed on $\text{Bi}_2\text{Sr}_2\text{CaCu}_2\text{O}_{8+\delta}$ in the

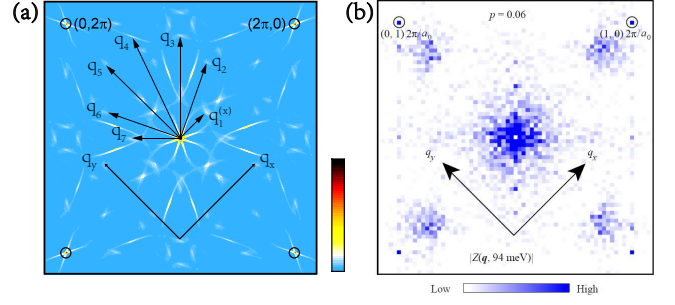


FIG. 1: (Color online) (a) The ARPES autocorrelation pattern in momentum-space in the binding-energy $\omega = 94$ meV for the strength of the electronic nematicity $\zeta = 0.006$. (b) The corresponding experimental result of the quasiparticle scattering interference pattern of $\text{Bi}_2\text{Sr}_2\text{CaCu}_2\text{O}_{8+\delta}$ in the binding-energy $\omega = 94$ meV at doping $\delta = 0.06$ taken from Ref. 28.

bind-energy $\omega = 94$ meV at doping $\delta = 0.06$ is also shown in Fig. 1b. The results in Fig. 1 thus show that the momentum-space structure of the ARPES autocorrelation pattern in the SC-state with coexisting electronic nematicity is qualitative consistent with the corresponding momentum-space structure of the QSI pattern observed on $\text{Bi}_2\text{Sr}_2\text{CaCu}_2\text{O}_{8+\delta}$. Moreover, the characteristic features of two distinct classes of the broken-symmetry states have been summarized as³⁹: (i) For the quasiparticle scattering processes with the corresponding scattering wave vectors $\mathbf{q}_1, \mathbf{q}_4,$ and \mathbf{q}_5 , the amplitudes of the quasiparticle scattering wave vectors are respectively inequivalent to their symmetry-corresponding partners, while for the quasiparticle scattering process with the corresponding quasiparticle scattering wave vectors $\mathbf{q}_2, \mathbf{q}_3, \mathbf{q}_6,$ and \mathbf{q}_7 , the scattering wave vectors and their symmetry-equivalent partners occur with equal amplitudes. These results therefore indicate that the peaks at the corresponding scattering wave vectors $\mathbf{q}_1, \mathbf{q}_4,$ and \mathbf{q}_5 are the signatures of the electronically ordered states with broken both rotation and translation symmetries, while the peaks with the corresponding scattering wave vectors $\mathbf{q}_2, \mathbf{q}_3, \mathbf{q}_6,$ and \mathbf{q}_7 are the signatures of the electronically ordered states with broken translation symmetry only; (ii) The intensity of the peak at the Bragg wave vector $\mathbf{Q}_x^{(B)}$ is different from that at the Bragg wave vector $\mathbf{Q}_y^{(B)}$. This difference leads to the inequivalence on the average of the electronic structure at the two Bragg scattering sites $\mathbf{Q}_x^{(B)}$ and $\mathbf{Q}_y^{(B)}$, and therefore shows that the Bragg peaks at the wave vectors $\mathbf{Q}_x^{(B)}$ and $\mathbf{Q}_y^{(B)}$ are the signature of the nematic-order state with the broken C_4 rotation symmetry.

We are now ready to discuss the doping dependence of the nematic-order state characteristic energy and of its possible connection to the enhancement of superconductivity. In our previous studies³⁹, the order parameter of

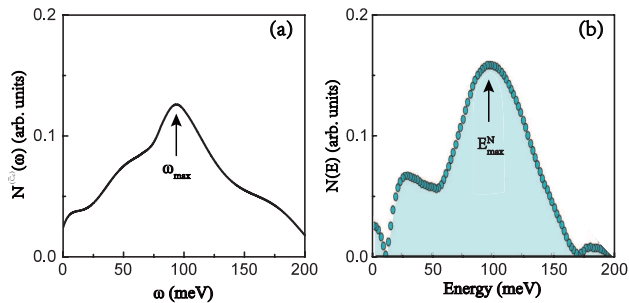


FIG. 2: (Color online) (a) The order parameter of the nematic-order state as a function of energy for the strength of the electronic nematicity $\zeta = 0.006$, where the arrow indicates the position of the peak at the characteristic energy. (b) The corresponding experimental result observed on $\text{Bi}_2\text{Sr}_2\text{CaCu}_2\text{O}_{8+\delta}$ at doping $\delta = 0.06$ taken from Ref. 28.

the electronic nematicity has been given as,

$$N^{(\bar{C}_\zeta)}(\omega) = \frac{\bar{C}_\zeta^{(x)}(\omega) - \bar{C}_\zeta^{(y)}(\omega)}{\bar{C}_\zeta^{(x)}(\omega) + \bar{C}_\zeta^{(y)}(\omega)}, \quad (13)$$

where $\bar{C}_\zeta^{(x)}(\omega) = (1/N) \sum_{\mathbf{q} \in \{\mathbf{Q}_x^{(B)}\}} \bar{C}_\zeta(\mathbf{q}, \omega)$ and $\bar{C}_\zeta^{(y)}(\omega) = (1/N) \sum_{\mathbf{q} \in \{\mathbf{Q}_y^{(B)}\}} \bar{C}_\zeta(\mathbf{q}, \omega)$, with the summation $\mathbf{q} \in \{\mathbf{Q}_x^{(B)}\} [\mathbf{q} \in \{\mathbf{Q}_y^{(B)}\}]$ that is restricted to the extremely small area $\{\mathbf{Q}_x^{(B)}\} [\{\mathbf{Q}_y^{(B)}\}]$ at around $\mathbf{Q}_x^{(B)} [\mathbf{Q}_y^{(B)}]$. This definition in Eq. (13) is confronted with the reduction of the size effect in a finite-lattice calculation. This follows a basic fact that the calculation for the normal and anomalous self-energies in Eq. (11) is performed numerically on a 120×120 lattice in momentum space as we have mentioned above, with the infinitesimal $i0_+ \rightarrow i\Gamma$ replaced by a small damping $\Gamma = 0.05J$, which leads to that the peak weight of the ARPES auto-correlation $\bar{C}_\zeta(\mathbf{q}, \omega)$ in Eq. (2) at the Bragg wave vector $\mathbf{Q}_x^{(B)} [\mathbf{Q}_y^{(B)}]$ spreads on the extremely small area $\{\mathbf{Q}_x^{(B)}\} [\{\mathbf{Q}_y^{(B)}\}]$ at around the $\mathbf{Q}_x^{(B)} [\mathbf{Q}_y^{(B)}]$ point. The summation of these spread weights in $\bar{C}_\zeta^{(x)}(\omega) [\bar{C}_\zeta^{(y)}(\omega)]$ at around this extremely small area $\{\mathbf{Q}_x^{(B)}\} [\{\mathbf{Q}_y^{(B)}\}]$ can reduce the size effect in the finite-lattice calculation. If this order parameter $N^{(\bar{C}_\zeta)}(\omega)$ is non-zero, the break of the C_4 rotation symmetry is occurring. In Fig. 2a, we plot the order parameter of the nematic-order state $N^{(\bar{C}_\zeta)}(\omega)$ as a function of binding-energy for the strength of the electronic nematicity $\zeta = 0.006$. For a direct comparison, the corresponding experimental result²⁸ of the energy dependence of the nematic-order state order parameter observed on $\text{Bi}_2\text{Sr}_2\text{CaCu}_2\text{O}_{8+\delta}$ at doping $\delta = 0.06$ is also shown in Fig. 2b. It thus shows clearly that the experimental result²⁸ of the energy dependence of the nematic-order state order parameter is well reproduced, where $N^{(\bar{C}_\zeta)}(\omega)$ reaches its maximum in the characteristic energy ω_{\max} , however, when the energy is turned away from this characteristic energy ω_{\max} , $N^{(\bar{C}_\zeta)}(\omega)$ drops rapidly. Moreover, this anticipated characteristic energy

$\omega_{\max} \sim 0.936J = 93.6$ meV is well consistent with the experimental result²⁸ of $E_{\max}^{(N)} \sim 94$ meV observed on $\text{Bi}_2\text{Sr}_2\text{CaCu}_2\text{O}_{8+\delta}$ at doping $\delta = 0.06$. This energy dependence of $N^{(\bar{C}_\zeta)}(\omega)$ with non-zero values therefore further verifies the nematic-order state with broken C_4 rotation symmetry in a wide energy range.

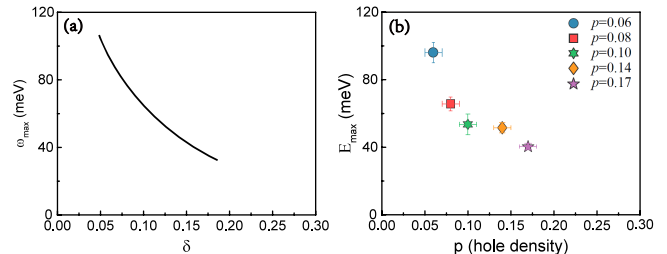


FIG. 3: (Color online) (a) The characteristic energy of the nematic-order state as a function of doping for the strength of the electronic nematicity $\zeta = 0.006$. (b) The corresponding experimental result observed on $\text{Bi}_2\text{Sr}_2\text{CaCu}_2\text{O}_{8+\delta}$ taken from Ref. 28.

As a natural consequence of the doped Mott insulators, the characteristic energy of the nematic-order state ω_{\max} also evolve strongly with doping. For a better understanding of the doping dependence of ω_{\max} , we plot the result of ω_{\max} as a function of doping for the strength of the electronic nematicity $\zeta = 0.006$ in Fig. 3a in comparison with the corresponding experimental result²⁸ of the doping dependence of the nematic-order state characteristic energy observed on $\text{Bi}_2\text{Sr}_2\text{CaCu}_2\text{O}_{8+\delta}$ in Fig. 3b. The result in Fig. 3a indicates clearly that ω_{\max} is particularly large in the underdoped regime, and then monotonically decreases as doping is increased, which is fully consistent with the corresponding result observed on $\text{Bi}_2\text{Sr}_2\text{CaCu}_2\text{O}_{8+\delta}$. Moreover, we have also compared the above result of the doping dependence of the nematic-order state characteristic energy with the experimental result of the doping dependence of the pseudogap²⁸, and found that the nematic-order state characteristic energy and pseudogap energy are also identical. The pseudogap in the framework of the kinetic-energy-driven superconductivity originates from the electron self-energy resulting of the dressing of the electrons due to the electron interaction mediated by a strongly dispersive spin excitation^{56–59}, and then it can be identified as being a region of the electron self-energy effect^{60,61} in which the pseudogap suppresses strongly the electronic density of states. The characteristic energy of the nematic-order state in theory and experiment is virtually identical to each other and also to the corresponding pseudogap energy. These results therefore are important to confirm the nematic-order state characteristic energy at the C_4 rotation symmetry-breaking can be understood as the natural consequence of the electronic nematic-order state within the pseudogap of cuprate superconductors²⁸.

In our recent studies³⁹, the evolution of T_c with the strength of the electronic nematicity has been obtained

within the framework of the kinetic-energy-driven superconductivity in terms of the self-consistent calculation at the condition of the SC gap $\bar{\Delta}^{(\zeta)} = 0$, where the optimized T_c at the optimal doping $\delta \approx 0.15$ increases with the increase of the strength of the electronic nematicity, and reaches its maximum in the optimal strength of the electronic nematicity $\zeta \approx 0.022$, subsequently, the optimized T_c decreases with the increase of the strength of the electronic nematicity in the strong strength region. This dome-like shape nematic-order strength dependence of T_c therefore shows clearly that superconductivity in cuprate superconductors is enhanced by the electronic nematicity. In particular, it has been shown that the energy in the SC-state with coexisting electronic nematicity is lower than the corresponding energy in the SC-state with the absence of the electronic nematicity³⁹. Moreover, the SC condensation energy as a function of the nematic-order state strength shows the same behavior of T_c . This same dome-like shape nematic-order strength dependence of the SC condensation energy thus leads to that superconductivity is enhanced by the electronic nematicity, and T_c exhibits a dome-like shape nematic-order strength dependence.

Now we turn our attention to the possible connection between the nematic-order state characteristic energy and the enhancement of superconductivity. To show this possible connection more clearly, we plot (a) ω_{\max} and (b) T_c as a function of the strength of the electronic nematicity ζ at the *underdoping* $\delta = 0.06$ in Fig. 4. In order to compare clearly the present results of the nematic-order state strength dependence of ω_{\max} and T_c with the corresponding results at different doping levels, the previous results³⁹ of (c) ω_{\max} and (d) T_c as a function of the strength of the electronic nematicity at the *optimal doping* $\delta = 0.15$ are also shown in Fig. 4. Obviously, two characteristic features in Fig. 4 can be summarized as: (i) for the present case at the underdoping $\delta = 0.06$ (see Fig. 4a and Fig. 4b), the strength range together with the *optimal strength* in ω_{\max} are the same with that in T_c . In particular, with the increase of the nematic-order state strength, ω_{\max} (then T_c) is raised gradually in the weak strength region, and achieves its maximum at around the *optimal strength* $\zeta = 0.022$. However, with the further increase of the strength, ω_{\max} (then T_c) turns into a monotonically decrease in the strong strength region; (ii) In comparison with the results³⁹ at the optimal doping $\delta = 0.15$ (see Fig. 4c and Fig. 4d), ω_{\max} in Fig. 4a (T_c in Fig. 4b) for a given nematic-order state strength at the underdoping $\delta = 0.06$ is much larger (lower) than the corresponding ω_{\max} in Fig. 4c (T_c in Fig. 4d) at the optimal doping $\delta = 0.15$. However, the global dome-like shape of the nematic-order strength dependence of ω_{\max} and T_c at the underdoping $\delta = 0.06$ together with the magnitude of the *optimal strength* are the same with that at the optimal doping $\delta = 0.15$. Therefore the enhancement of superconductivity occurs at a any given doping of the SC dome. This same strength range together with the same *optimal strength* in the characteristic energy

ω_{\max} and SC transition temperature T_c therefore indicates firstly a possible connection between the nematic-order state characteristic energy and the enhancement of superconductivity.

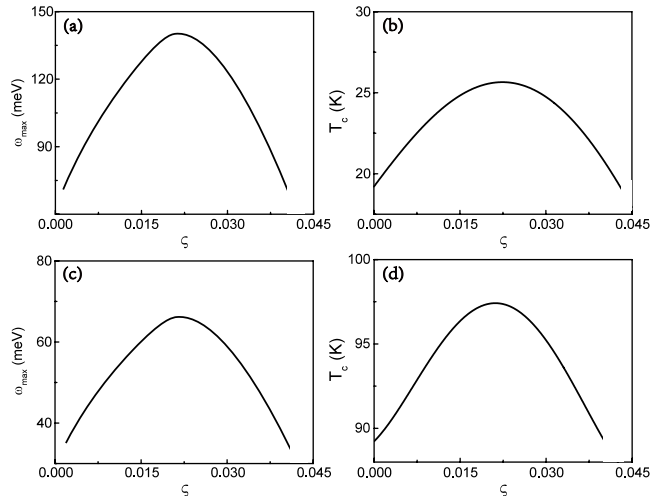


FIG. 4: (Color online) (a) The nematic-order state characteristic energy as a function of the strength of the electronic nematicity ζ at the underdoping $\delta = 0.06$. (b) The superconducting transition temperature as a function of the strength of the electronic nematicity at the underdoping $\delta = 0.06$. The corresponding results of (c) the nematic-order state characteristic energy as a function of the strength of the electronic nematicity ζ at the optimal doping $\delta = 0.15$ and (d) the superconducting transition temperature as a function of the strength of the electronic nematicity at the optimal doping $\delta = 0.15$ taken from Ref. 39.

IV. SUMMARY AND DISCUSSIONS

Within the framework of the kinetic-energy-driven superconductivity, we have studied the doping dependence of the nematic-order state characteristic energy in cuprate superconductors and of its possible connection to the enhancement of superconductivity. Our results show clearly that the characteristic energy of the nematic-order state is particularly large in the underdoped regime, then it smoothly decreases as doping is increased, in full agreement with the corresponding to the STS experimental observations. More importantly, our results also indicate firstly that the characteristic energy of the nematic-order state as a function of the nematic-order state strength in the underdoped regime presents a similar behavior of the SC transition temperature. On the basis of these obtained results, the theory therefore predicts a possible connection between the nematic-order state characteristic energy and the enhancement of superconductivity.

Finally, it should be noted that apart from the emergence of the electronically nematic order in cuprate superconductors⁷⁻⁹, the electronic nematicity has been observed across several families of

strongly correlated electron systems, including iron-based superconductors^{62–64}, strontium ruthenates⁶⁵, kagome lattice materials⁶⁶, heavy fermion systems⁶⁷, as well as nickel-based superconductors⁶⁸. In particular, in the context of iron-based superconductors^{62–64}, the experimental observations have shown a striking enhancement of nematic fluctuations centred at optimal tuning of superconductivity. Moreover, the nematic-fluctuation-enhanced superconductivity in nickel-based superconductors has been observed experimentally⁶⁸. In a strongly correlated electron system, the strong electron correlation induces the system to find new way to lower its total energy, often by spontaneous breaking of the native symmetries of the lattice. These experimental observations^{62–68} together with the experimental detection in cuprate superconductors^{7–9} therefore indicate that the electronic nematicity is a common phenomenon

in strongly correlated electron systems, and then a characteristic feature in the complicated phase diagram is the interplay between the electronic nematicity and superconductivity.

Acknowledgements

ZC, XM, and SF are supported by the National Key Research and Development Program of China, and the National Natural Science Foundation of China (NSFC) under Grant Nos. 11974051 and 11734002. HG is supported by NSFC under Grant Nos. 11774019 and 12074022, and the Fundamental Research Funds for the Central Universities and HPC resources at Beihang University.

-
- * Electronic address: spfeng@bnu.edu.cn
- ¹ J. G. Bednorz and K. A. Müller, *Z. Phys. B* **64**, 189 (1986).
 - ² See, e.g., the review, S. L. Cooper and K. E. Grey, in *Physical Properties of High Temperature Superconductors IV*, edited by D. M. Ginsberg (World Scientific, Singapore, 1994), p. 61.
 - ³ K. Takenaka, K. Mizunashi, H. Takagi, and S. Uchida, *Phys. Rev. B* **50**, 6534(R) (1994).
 - ⁴ See, e.g., the review, I. M. Vishik, *Rep. Prog. Phys.* **81**, 062501 (2018).
 - ⁵ See, e.g., the review, R. Comin and A. Damascelli, *Annu. Rev. Condens. Matter Phys.* **7**, 369 (2016).
 - ⁶ S. A. Kivelson and S. Lederer, *Proc. Natl. Acad. Sci.* **116**, 14395 (2019).
 - ⁷ See, e.g., the review, Matthias Vojta, *Adv. Phys.* **58**, 699 (2009).
 - ⁸ See, e.g., the review, E. Fradkin, S. A. Kivelson, M. J. Lawler, J. P. Eisenstein, and A. P. Mackenzie, *Annu. Rev. Condens. Matter Phys.* **1**, 153 (2010).
 - ⁹ See, e.g., the review, R. M. Fernandes, P. P. Orth, and J. Schmalian, *Annu. Rev. Condens. Matter Phys.* **10**, 133 (2019).
 - ¹⁰ S. Nakata, M. Horio, K. Koshiishi, K. Hagiwara, C. Lin, M. Suzuki, S. Ideta, K. Tanaka, D. Song, Y. Yoshida, H. Eisaki, A. Fujimori, *npj Quantum Mater.* **6**, 86 (2021).
 - ¹¹ V. Hinkov, D. Haug, B. Fauqué, P. Bourges, Y. Sidis, A. Ivanov, C. Bernhard, C. T. Lin, B. Keimer, *Science* **319**, 597 (2008).
 - ¹² Y. Sato, S. Kasahara, H. Murayama, Y. Kasahara, E.-G. Moon, T. Nishizaki, T. Loew, J. Porras, B. Keimer, T. Shibauchi, and Y. Matsuda, *Nat. Phys.* **13**, 1074 (2017).
 - ¹³ R. Daou, J. Chang, D. LeBoeuf, O. Cyr-Choinière, F. Laliberté, N. Doiron-Leyraud, B. J. Ramshaw, R. Liang, D. A. Bonn, W. N. Hardy, and L. Taillefer, *Nature* **463**, 519 (2010).
 - ¹⁴ O. Cyr-Choinière, G. Grissonnanche, S. Badoux, J. Day, D. A. Bonn, W. N. Hardy, R. Liang, N. Doiron-Leyraud, and L. Taillefer, *Phys. Rev. B* **92**, 224502 (2015).
 - ¹⁵ W. Wang, J. Luo, C. G. Wang, J. Yang, Y. Kodama, R. Zhou, G.-Q. Zheng, *Sci. China-Phys. Mech. Astron.* **64**, 237413 (2021).
 - ¹⁶ Y. Ando, K. Segawa, S. Komiya, and A. N. Lavrov, *Phys. Rev. Lett.* **88**, 137005 (2002).
 - ¹⁷ J. Wu, A. T. Bollinger, X. He, and I. Božović, *Nature* **547**, 432 (2017).
 - ¹⁸ M. J. Lawler, K. Fujita, J. Lee, A. R. Schmidt, Y. Kohsaka, C. K. Kim, H. Eisaki, S. Uchida, J. C. Davis, J. P. Sethna, and E.-A. Kim, *Nature* **466**, 347 (2010).
 - ¹⁹ K. Fujita, C. K. Kim, I. Lee, J. Lee, M. H. Hamidian, I. A. Firmo, S. Mukhopadhyay, H. Eisaki, S. Uchida, M. J. Lawler, E.-A. Kim, J. C. Davis, *Science* **344**, 612 (2014).
 - ²⁰ Y. Zheng, Y. Fei, K. Bu, W. Zhang, Y. Ding, X. J. Zhou, J. E. Hoffman, and Y. Yin, *Sci. Rep.* **7**, 8059 (2017).
 - ²¹ T. Wu, H. Mayaffre, S. Krämer, M. Horvatić, C. Berthier, W. N. Hardy, R. Liang, D. A. Bonn, and M.-H. Julien, *Nature* **477**, 191 (2011).
 - ²² R. Comin, A. Frano, M. M. Yee, Y. Yoshida, H. Eisaki, E. Schierle, E. Weschke, R. Sutarto, F. He, A. Soumyanarayanan, Y. He, M. Le Tacon, I. S. Elfimov, J. E. Hoffman, G. A. Sawatzky, B. Keimer and A. Damascelli, *Science* **343**, 390 (2014).
 - ²³ S. Gerber, H. Jang, H. Nojiri, S. Matsuzawa, H. Yasumura, D. A. Bonn, R. Liang, W. N. Hardy, Z. Islam, A. Mehta, S. Song, M. Sikorski, D. Stefanescu, Y. Feng, S. A. Kivelson, T. P. Devereaux, Z.-X. Shen, C.-C. Kao, W.-S. Lee, D. Zhu, and J.-S. Lee, *Science* **350**, 949 (2015).
 - ²⁴ Y. Y. Peng, M. Salluzzo, X. Sun, A. Ponti, D. Betto, A. M. Ferretti, F. Fumagalli, K. Kummer, M. Le Tacon, X. J. Zhou, N. B. Brookes, L. Braicovich, and G. Ghiringhelli, *Phys. Rev. B* **94**, 184511 (2016).
 - ²⁵ S. Caprara, C. Di Castro, G. Seibold, and M. Grilli, *Phys. Rev. B* **95**, 224511 (2017).
 - ²⁶ R. Arpaia, S. Caprara, R. Fumagalli, G. De Vecchi, Y. Y. Peng, E. Andersson, D. Betto, G. M. De Luca, N. B. Brookes, F. Lombardi, M. Salluzzo, L. Braicovich, C. Di Castro, M. Grilli, G. Ghiringhelli, *Science* **365**, 906 (2019).
 - ²⁷ E. Wahlberg, R. Arpaia, G. Seibold, M. Rossi, R. Fumagalli, E. Tralbaldo, N. B. Brookes, L. Braicovich, S. Caprara, U. Gran, G. Ghiringhelli, T. Bauch, F. Lombardi, *Science* **373**, 1506 (2021).
 - ²⁸ S. Mukhopadhyay, R. Sharma, C. K. Kim, S. D. Ekins, M. H. Hamidian, H. Eisaki, S. Uchida, E.-A. Kim, M. J.

- Lawler, A. P. Mackenzie, J. C. S. Davis, and K. Fujita, Proc. Natl. Acad. Sci. **116**, 13249 (2019).
- ²⁹ S. A. Kivelson, E. Fradkin, and V. J. Emery, Nature **393**, 550 (1998).
- ³⁰ J. Zaanen, Physica C **317-318**, 217 (1999).
- ³¹ S. A. Kivelson, I. P. Bindloss, E. Fradkin, V. Oganesyan, J. M. Tranquada, A. Kapitulnik, and C. Howald, Rev. Mod. Phys. **75**, 1201 (2003).
- ³² L. Nie, L. E. H. Sierens, R. G. Melko, S. Sachdev, and S. A. Kivelson, Phys. Rev. B **92**, 174505 (2015).
- ³³ C. J. Halboth and W. Metzner, Phys. Rev. Lett. **85**, 5162 (2000).
- ³⁴ M. Kitatani, N. Tsuji, and H. Aoki, Phys. Rev. B **95**, 075109 (2017).
- ³⁵ Z. Dai, Y.-H. Zhang, T. Senthil, and P. A. Lee, Phys. Rev. B **97**, 174511 (2018).
- ³⁶ W. L. Tu and T. K. Lee, Sci. Rep. **9**, 1719 (2019).
- ³⁷ N. Auvray, B. Lorent, S. Benhabib, M. Cazayous, R. D. Zhong, J. Schneeloch, G. D. Gu, A. Forget, D. Colson, I. Paul, A. Sacuto, and Y. Gallais, Nat. Commun. **10**, 5209 (2019).
- ³⁸ S. Bulut, W. A. Atkinson, and A. P. Kampf, Phys. Rev. B **88**, 155132 (2013).
- ³⁹ Z. Cao, Y. Liu, H. Guo, and S. Feng, arXiv:2105.14494.
- ⁴⁰ S. H. Pan, J. P. ÓNeal, R. L. Badzey, C. Chamon, H. Ding, J. R. Engelbrecht, Z. Wang, H. Eisaki, S. Uchida, A. K. Gupta, K.-W. Ng, E. W. Hudson, K. M. Lang, and J. C. Davis, Nature **413**, 282 (2001).
- ⁴¹ See, e.g., the review, Ø. Fischer, M. Kugler, I. Maggio-Aprile, C. Berthod, and C. Renner, Rev. Mod. Phys. **79**, 353 (2007).
- ⁴² See, e.g., the review, J.-X. Yin, S. H. Pan, M. Z. Hasan, Nat. Rev. Phys. **3**, 249 (2021).
- ⁴³ D. Gao, Y. Mou, Y. Liu, S. Tan, and S. Feng, Phil. Mag. **99**, 752 (2019).
- ⁴⁴ Q.-H. Wang and D.-H. Lee, Phys. Rev. B **67**, 020511 (2003).
- ⁴⁵ U. Chatterjee, M. Shi, A. Kaminski, A. Kanigel, H. M. Fretwell, K. Terashima, T. Takahashi, S. Rosenkranz, Z. Li, H. Raffy, A. Santander-Syro, K. Kadowaki, M. R. Norman, M. Randeria, and J. C. Campuzano, Phys. Rev. Lett. **96**, 107006 (2006).
- ⁴⁶ Y. He, Y. Yin, M. Zech, A. Soumyanarayanan, M. M. Yee, T. Williams, M. C. Boyer, K. Chatterjee, W. D. Wise, I. Zeljkovic, T. Kondo, T. Takeuchi, H. Ikuta, P. Mistark, R. S. Markiewicz, A. Bansil, S. Sachdev, E. W. Hudson, J. E. Hoffman, Science **344**, 608 (2014).
- ⁴⁷ P. W. Anderson, Science **235**, 1196 (1987).
- ⁴⁸ Ying-Jer Kao and Hae-Young Kee, Phys. Rev. B **72**, 024502 (2005).
- ⁴⁹ B. Edegger, V. N. Muthukumar, and C. Gros, Phys. Rev. B **74**, 165109 (2006).
- ⁵⁰ A. Wollny and M. Vojta, Physica B **404**, 3079 (2009).
- ⁵¹ K. Lee, S. A. Kivelson, and E.-A. Kim, Phys. Rev. B **94**, 014204 (2016).
- ⁵² S. Feng, J. B. Wu, Z. B. Su, and L. Yu, Phys. Rev. B **47**, 15192 (1993).
- ⁵³ See, e.g., the review, L. Yu, in *Recent Progress in Many-Body Theories*, edited by T. L. Ainsworth, C. E. Campbell, B. E. Clements, and E. Krotscheck (Plenum, New York, 1992), Vol. **3**, p. 157.
- ⁵⁴ See, e.g., the review, P. A. Lee, N. Nagaosa, and X.-G. Wen, Rev. Mod. Phys. **78**, 17 (2006).
- ⁵⁵ S. Feng, J. Qin, and T. Ma, J. Phys.: Condens. Matter **16**, 343 (2004); S. Feng, Z. B. Su, and L. Yu, Phys. Rev. B **49**, 2368 (1994).
- ⁵⁶ See, e.g., the review, S. Feng, Y. Lan, H. Zhao, L. Kuang, L. Qin, and X. Ma, Int. J. Mod. Phys. B **29**, 1530009 (2015).
- ⁵⁷ S. Feng, Phys. Rev. B **68**, 184501 (2003); S. Feng, T. Ma, and H. Guo, Physica C **436**, 14 (2006).
- ⁵⁸ S. Feng, H. Zhao, and Z. Huang, Phys. Rev. B **85**, 054509 (2012); Phys. Rev. B **85**, 099902(E) (2012).
- ⁵⁹ S. Feng, L. Kuang, and H. Zhao, Physica C **517**, 5 (2015).
- ⁶⁰ See, e.g., the review, T. Timusk and B. Statt, Rep. Prog. Phys. **62**, 61 (1999).
- ⁶¹ See, e.g., the review, S. Hüfner, M. A. Hossain, A. Damascelli, and G. A. Sawatzky, Rep. Prog. Phys. **71**, 062501 (2008).
- ⁶² T.-M. Chuang, M. P. Allan, J. Lee, Y. Xie, N. Ni, S. L. Budko, G. S. Boebinger, P. C. Canfield, J. C. Davis, Science **327**, 181 (2010).
- ⁶³ Y. Gallais, R. M. Fernandes, I. Paul, L. Chauvière, Y.-X. Yang, M.-A. Méasson, M. Cazayous, A. Sacuto, D. Colson, and A. Forget, Phys. Rev. Lett. **111**, 267001 (2013).
- ⁶⁴ P. Massat, D. Farina, I. Paul, S. Karlsson, P. Strobel, P. Toulemonde, M.-A. Méasson, M. Cazayous, A. Sacuto, S. Kasahara, T. Shibauchi, Y. Matsuda, and Y. Gallais, Proc. Natl. Acad. Sci. **113**, 9177 (2016).
- ⁶⁵ R. A. Borzi, S. A. Grigera, J. Farrell, R. S. Perry, S. J. S. Lister, S. L. Lee, D. A. Tennant, Y. Maeno, and A. P. Mackenzie, Science **315**, 214 (2007).
- ⁶⁶ J. X. Yin, S. S. Zhang, H. Li, K. Jiang, G. Chang, B. Zhang, B. Lian, C. Xiang, I. Belopolski, H. Zheng, T. A. Cochran, S. Y. Xu, G. Bian, K. Liu, T. R. Chang, H. Lin, Z. Y. Lu, Z. Wang, S. Jia, W. Wang and M. Z. Hasan, Nature **562**, 91 (2018).
- ⁶⁷ R. Okazaki, T. Shibauchi, H. J. Shi, Y. Haga, T. D. Matsuda, E. Yamamoto, Y. Onuki, H. Ikeda, Y. Matsuda, Science **331**, 439 (2011).
- ⁶⁸ C. Eckberg, D. J. Campbell, T. Metz, J. Collini, H. Hodovanets, T. Drye, P. Zavalij, M. H. Christensen, R. M. Fernandes, S. Lee, P. Abbamonte, J. W. Lynn, and J. Paglione, Nat. Phys. **16**, 346 (2020).